Title: Climate predicts geographic and temporal variation in mosquito-borne disease dynamics on two continents

Jamie M. Caldwell[1], A. Desiree LaBeaud[2], Eric F. Lambin[3,4], Anna M. Stewart-Ibarra[5,6], Bryson A. Ndenga[7], Francis M. Mutuku[8], Amy R. Krystosik[2], Efraín Beltrán Ayala[9], Assaf Anyamba[10], Mercy J. Borbor-Cordova[11], Richard Damoah[12], Elysse N. Grossi-Soyster[2], Froilán Heras Heras[13], Harun N. Ngugi[14,15], Sadie J. Ryan[16-18], Melisa M. Shah[19], Rachel Sippy[13,20,21], Erin A. Mordecai[1]

[1] Department of Biology, Stanford University, 371 Serra Mall, Stanford, California, USA

[2] Department of Pediatrics, Division of Infectious Diseases, Stanford University, 300 Pasteur Drive, Stanford, California, USA

[3] School of Earth, Energy & Environmental Sciences, and Woods Institute for the Environment, Stanford University, Stanford, California 94305, USA.

[4] Georges Lemaître Earth and Climate Research Centre, Earth and Life Institute, Université catholique de Louvain, 1348 Louvain-la-Neuve, Belgium.

[5] Department of Medicine and Department of Public Health and Preventative Medicine, SUNY Upstate Medical University, Syracuse, NY, USA

[6] InterAmerican Institute for Global Change Research (IAI), Montevideo, Uruguay

[7] Centre for Global Health Research, Kenya Medical Research Institute, Kisumu, Kenya

[8] Department of environment and health sciences, technical university of Mombasa, Mombasa, Kenya

[9] Technical University of Machala, Machala, Ecuador

[10] Universities Space Research Association and NASA Goddard Space Flight Center, Greenbelt, MD, USA.

[11] Facultad de Ingeniería Marítima y Ciencias del Mar, Escuela Superior Politécnica del Litoral, ESPOL, Guayaquil, Ecuador

[12] Morgan State University and NASA Goddard Space Flight Center, Greenbelt, MD, USA.

[13] Center for Research SUNY-Upstate-Teófilo Dávila Hospital, Machala, Ecuador

[14] Department of Biological Sciences, Chuka University, Chuka, Kenya

[15] Department of Zoology, School of Biological Sciences University of Nairobi, Nairobi, Kenya

[16] Emerging Pathogens Institute, University of Florida, Gainesville, Florida

[17] Quantitative Disease Ecology and Conservation (QDEC) Lab, Department of Geography, University of Florida, Gainesville, Florida;

[18] School of Life Sciences, University of KwaZulu, Natal, South Africa

[19] Department of Medicine, Division of Infectious Diseases, Stanford University, 300 Pasteur Drive, Stanford, California, USA

[20] Institute for Global Health and Translational Science, SUNY-Upstate Medical University, Syracuse, NY, USA

[21] Department of Medical Geography, University of Florida, Gainesville, FL, USA

Corresponding author email: jamie.sziklay@gmail.com

Abstract:

Climate drives population dynamics through multiple mechanisms, which can lead to seemingly context-dependent effects of climate on natural populations. For climate-sensitive diseases such as dengue, chikungunya, and Zika, climate appears to have opposing effects in different contexts. Here we show that a model, parameterized with laboratory measured climate-driven mosquito physiology, captures three key epidemic characteristics across ecologically and culturally distinct settings in Ecuador and Kenya: the number, timing, and duration of outbreaks. The model generates a range of disease dynamics consistent with observed *Aedes aegypti* abundances and laboratory-confirmed arboviral incidence with variable accuracy (28 – 85% for vectors, 44 – 88% for incidence). The model predicted vector dynamics better in sites with a smaller proportion of young children in the population, lower mean temperature, and homes with piped water and made of cement. Models with limited calibration that robustly capture climate-virus relationships can help guide intervention efforts and climate change disease projections.

Introduction:

Climate is a major driver of species interactions and population dynamics, but the mechanisms underlying the ecological effects of climate are often poorly understood and rarely tested in the field [1]. One of the primary ways that climate impacts populations is through its effects on species' vital rates [2]. However, the effects of climate on population dynamics may appear context dependent in the field because multiple climate variables can act synergistically, with each climate variable potentially affecting multiple

vital rates, and their impacts may be nonlinear, changing direction and relative importance across a gradient of conditions [3,4]. Therefore, paradoxically, while climate is thought to be one of the most pervasive drivers of ecological processes, its directional and dynamical effects on systems are often poorly understood and difficult to predict. Vector-borne diseases provide an interesting case study to test whether climate sensitive traits measured in controlled, laboratory settings can reproduce the wide range of dynamics observed in the field. For example, transmission of mosquito-borne viral (arboviral) diseases such as dengue, chikungunya, and Zika occur along a spectrum from low levels of year-round endemic transmission [5] to large seasonal or interannual outbreaks [6]. We hypothesize that important features of these differing dynamics arise due to regional or seasonal differences in climate, where the magnitude and direction of the effects of climate on vector and disease dynamics differ [7–12].

Understanding the mechanisms that drive disease dynamics can help address two critically important research priorities for arboviruses like dengue, chikungunya, and Zika: assessing intervention strategies and projecting climate change impacts on disease dynamics. While phenomenological models often replicate arboviral disease dynamics remarkably well [13], mechanistic models that do not rely on local data for calibration and capture mosquito population dynamics and interactions between mosquitoes and humans will provide more realistic projections for epidemic dynamics across a broad range of transmission settings. With no widely available vaccine, vector control (e.g., larvicides, *Wolbachia*-infected mosquito releases) remains the primary method for preventing arboviral disease transmission, and, like other vector-borne diseases with

93 complex transmission dynamics, model simulations can help guide effective intervention
94 efforts [14,15]. Further, mechanistic models are better suited to predict how climate
95 change will impact future disease burden and distribution, as projected climate conditions
96 are outside the current arboviral climate niche space [16]. Despite the potential usefulness
97 of mechanistic approaches, validation with vector and disease data are limited, raising an
98 important question about which epidemic characteristics, if any, we should expect a
99 model to capture when the model was parameterized with data that is on different scales
100 (e.g., individuals versus populations) and independent from the transmission system we
101 wish to predict. Thus, because we cannot study epidemic dynamics in every possible
102 transmission setting, it becomes important to understand the extent to which models
103 derived from fundamental and laboratory-measured traits explain disease dynamics
104 across diverse settings.
105
106 We hypothesize that a climate-driven mechanistic model with limited calibration should
107 capture many important characteristics of disease dynamics for dengue, chikungunya, and
108 Zika because of the ecology of *Aedes aegypti*, the primary disease vector. *Ae. aegypti* are
109 anthropophilic, globally distributed mosquitoes that breed in artificial containers with
110 standing water [17,18]. All mosquito and parasite traits that are important for
111 transmission and linked to metabolism, such as reproduction, development, survival,
112 biting rate, and extrinsic incubation period, are temperature dependent with an
113 intermediate thermal optimum [19–21]. Humidity is positively associated with mosquito
114 survival because the high surface area to volume ratio of mosquitoes exposes them to
115 desiccation [22,23]. Standing water from rainfall provides essential larval and pupal

116 habitat for mosquitoes, but the relationship is complex because heavy rainfall can flush
117 away breeding habitats [24–26] and water storage practices during drought can increase
118 water availability, mosquito abundance, and contact between mosquitoes and people [27–
119 29]. A previous simulation study predicted that in settings with suitable climate for
120 transmission throughout the year (e.g., mean temperature = 25°C; range = 20 – 30°C),
121 temperature drives the timing and duration of outbreaks, but not the maximum number of
122 infections or final epidemic size [30]. This finding suggests that a model that incorporates
123 temperature-dependent vector traits should capture some important epidemic
124 characteristics.
125
126 Arboviral dynamics differ considerably in South America and sub-Saharan Africa,
127 potentially because of differences in climate and socio-ecological conditions. Previous
128 studies have found that *Ae. aegypti* and dengue were positively associated with warm and
129 wet conditions in South America and sub-Saharan Africa [6,36–38], although other *Ae.*
130 *aegpyti*-vectored arboviruses in Africa such as chikungunya have been associated with
131 warm and dry conditions [39]. Countries on both continents have all four dengue
132 serotypes circulating and have recently experienced outbreaks of chikungunya; yet,
133 arboviral transmission dynamics differ in each region. In South America, dengue is a re-
134 emerging disease with large seasonal epidemics that frequently result in severe dengue
135 [6]; by contrast, in sub-Saharan Africa, dengue is transmitted at low levels year-round [5]
136 and intermittent self-limiting outbreaks often go undetected [40]. Further, compared with
137 South America, severe dengue is rare in sub-Saharan Africa, perhaps because African

138 strains of *Ae. aegpyti* have lower susceptibility to all four dengue serotypes [41], and/or
139 because people of African ancestry are less susceptible to severe dengue [42].
140
141 In this work, we test the extent to which climate-driven mosquito traits drive disease
142 dynamics across two geographically distinct regions and characterize additional
143 climatological, ecological, and social factors that may mediate the effects of climate on
144 disease dynamics. We build on previous mechanistic and semi-mechanistic models that
145 incorporate the *Aedes* mosquito life cycle and human disease dynamics [30–35] by
146 combining a suite of temperature, humidity, and rainfall dependent trait functions into
147 one epidemiological model. We validate the model with *Ae. aegypti* abundances and
148 laboratory-confirmed dengue, chikungunya, and Zika cases from two equatorial countries
149 with distinct socioeconomic, geographic, cultural, and disease transmission settings:
150 Ecuador and Kenya. We find that a climate-driven model with limited calibration to local
151 data captures three key epidemic characteristics across diverse settings: the number,
152 timing, and duration of outbreaks. The model generates a range of vector and disease
153 dynamics with varying levels of accuracy. Further, we find that the model predicted
154 vector dynamics better in sites with a smaller proportion of young children in the
155 population, lower mean temperature, and homes with piped water and made of cement.
156 These results indicate that a climate-driven model with limited calibration can capture
157 important epidemic characteristics, which can help guide intervention efforts and
158 improve disease projections associated with climate change.
159
160

Results:

Study sites

We selected study sites within each country that are distributed across a gradient of temperature, humidity, and rainfall and are climatologically and socio-economically distinct (Fig. 1, Table 1). The climate gradient is driven by factors like elevation, distance to ocean, and land cover type, as all study sites are located at similar latitudes near the equator. Demographics, housing quality, and exposure, susceptibility, and adaptive capacity vary most strongly between the two regions, although there are some differences among sites within the same the country.

Table 1: Study sites differ geographically, climatologically, and socioeconomically. [1]Mean annual normalized difference vegetation index (NDVI) is a proxy for photosynthesis and measured as a difference in spectral reflectance in the visible and near-infrared regions from NASA/NOAA MODIS (MOD13A1) [43]. [2]Dominant land cover type is measured and classified from spectral and temporal features from NASA/NOAA MODIS (MCD12Q1) [44]. Land cover types include (9) Tree cover 10 - 30%, (10) Dominated by herbaceous annuals, (13) >30% impervious surface area, and (14) 40 - 60% mosaics of small-scale cultivation. Bed net use represents availability of and/or willingness to adopt intervention strategies for preventing infection rather than a direct adaptive response to preventing infection by day-biting *Ae. aegpyti* mosquitoes.

	Huaquillas, Ecuador	Machala, Ecuador	Portovelo, Ecuador	Zaruma, Ecuador	Chulaimbo, Kenya	Kisumu, Kenya	Msmabweni, Kenya	Ukunda, Kenya
Site characteristics								
Elevation (m)	15	6	645	1,155	1,328	1,100	4	8
Location	Coastal	Coastal	Inland	Inland	Inland	Inland	Coastal	Coastal
Mean annual NDVI[1]	0.22	0.12	0.61	0.57	0.63	0.35	0.33	0.52
Dominant land cover type[2]	13	13	9	10	14	13	13	10
Climate								
Mean temperature (°C)	26	26	25	22	24	26	28	28
Mean relative humidity (%)	81	84	81	86	69	50	76	78
Mean annual rainfall (mm)	317	669	500	1115	1125	810	1048	922
Demographics								
Human population size	57,366	279,887	13,673	25,615	7,304	491,893	15,371	80,193
Population <5 years (%)	10	9	9	8	12	12	13	14
Population of African ancestry (%)	5.1	6.0	3.3	2.9	100.0	100.0	100.0	100.0
Housing quality (% houses)								
Piped water inside home	90	91	100	96	2	4	3	11
No screens on windows	7	60	91	99	74	78	43	21
House materials (cement/mud/wood)	87/5/0	87/8/5	95/0/5	93/1/1	29/70/0	77/17/0	38/62/0	51/47/0
Exposure, vulnerability, and adaptive capacity								
Arboviruses present	dengue, chikungunya, Zika				>200 documented including dengue, chikungunya, Yellow fever, Rift Valley fever, West Nile fever, O'nyong-nyong			
Insecticide use (% houses)	19	28	46	37	0	0	11	55
Bednet use (% houses)	77	55	15	21	93	92	0	96
Other vector control strategies used	Ultra-low volume fumigation with malathion (organophosphate) and community mobilization to eliminate larval habitats				Mosquito coils			
Annual gross domestic product by country (2018)	$177 billion USD				$85.98 billion USD			

183

184 Capturing key epidemic characteristics

185 The dynamic susceptible, exposed, infectious – susceptible, exposed, infectious, removed

186 (SEI-SEIR) compartmental model parameterized with temperature-, humidity-, and

187 rainfall-dependent mosquito life history traits (Fig. 2) reproduced three key

188 characteristics of epidemics: number of outbreaks, timing of outbreak peak, and duration

of outbreaks. We defined an outbreak as a continuous time period with peak cases exceeding the mean number of cases (predicted or observed) plus one standard deviation within a site. Across all sites, the number of outbreaks predicted by the model closely matched the number of outbreaks observed ($R^2 = 0.79$, $p < 0.01$; Fig. 3a). Supporting our *a priori* expectations based on a previous simulation study [30], we found that the climate-driven model predicted peak timing of outbreaks ($R^2 = 0.71$, $p < 0.01$; Fig. 3b) and outbreak duration ($R^2 = 0.51$, $p < 0.01$; Fig. 3c) well but did not predict the final outbreak size (Fig. 3d) or maximum number of infections (Fig. 3e) across sites. Overall, the model predicted four outbreaks that were not observed and did not predict five outbreaks that occurred. The model may miss an outbreak (i.e., false negatives) when, for example, suitable climate occurs but the pathogen is not introduced or the susceptible population is depleted from previous outbreaks.

Capturing spatio-temporal disease dynamics across sites

The SEI-SEIR model generated mosquito and disease dynamics that better reflected observed dynamics in some sites than others (Fig. 4, Table 2). Model-predicted mosquito abundances were significantly correlated with field-collected observations of mosquito abundances in all eight study sites, explaining 28 – 85% of site-level variation through time based on pairwise correlations with an adjusted p-value for time series data (following [45]). Based on surveys conducted across all vector life stages in Kenya (only adult mosquitoes were collected in the Ecuador surveys), the SEI-SEIR model explained variation in the abundance of adult mosquitoes (28 – 63%) better than pupae (25 – 32%), late instars (30 – 33%), early instars (20 – 36%), and eggs (33 – 55%), likely because the

model did not explicitly incorporate other mosquito life history stages. Model-predicted disease cases were significantly correlated with laboratory-confirmed arboviral incidence in seven of the eight study sites, explaining 44 – 88% of site-level variation through time (within sites with statistically significant pairwise correlations). We confirmed that the predicted dynamics were stable with sensitivity analyses to initial conditions (see Methods), as emerging diseases can display chaotic dynamics due to a high sensitivity to initial conditions. Overall, the model reproduced disease dynamics slightly better for sites in Ecuador compared with Kenya.

Table 2: Model predictions reflect a range of observed transmission dynamics when incorporating different rainfall functions and time lags across sites. For each study site, we calculated pairwise correlations between time series of field observations (*Ae. aegypti* abundances or arboviral cases) and time series of model predictions for the SEI-SEIR model with one of three rain functions for mosquito carrying capacity (Brière, Inverse, or Quadratic) and six time lags (0-5 months). This table shows specifications for the model (e.g., rain function and time lag) with the highest pairwise correlation value, r, for each study site and observation type (vectors or human disease cases), as well as the statistical significance of the correlation value (adjusted p-value for two-sided hypothesis test) based on the Modified Chelton method [45] to account for temporal autocorrelation.

	Vector dyanmics				Human disease dynamics			
Site	Rainfall function	r	Adjusted p-value	Lag (months)	Rainfall function	r	Adjusted p-value	Lag (months)
Huaquillas, Ecuador	Quadratic	0.63	0.01	1	Inverse	0.60	0.00	2
Machala, Ecuador	Quadratic	0.63	0.01	0	Brière	0.64	0.00	4
Portovelo, Ecuador	Brière	0.66	0.01	1	Brière	0.88	0.00	3
Zaruma, Ecuador	Inverse	0.85	0.00	1	Inverse	0.33	0.12	0
Chulaimbo, Kenya	Inverse	0.45	0.00	1	Quadratic	0.36	0.02	4
Kisumu, Kenya	Brière	0.48	0.00	0	Quadratic	0.51	0.00	4
Msambweni, Kenya	Inverse	0.28	0.04	0	Inverse	0.57	0.00	3
Ukunda, Kenya	Inverse	0.37	0.03	1	Inverse	0.78	0.00	5

We found evidence that rainfall affects transmission through multiple mechanisms and at different time lags (Table 2). Since the effect of rainfall on mosquito abundances is not

well understood, we simulated disease dynamics for each site three times, using one of three hypothesized rainfall relationships (Brière, inverse, and quadratic; Supplementary Fig. 3). We determined the best rainfall function and time lag for each site based on the highest pairwise correlation value between model predictions and observations. The model with the exponentially decreasing inverse rain function (Supplementary Fig. 3c), which indicates that mosquito abundances peak when there is no or low rainfall (likely as a result of water storage practices and/or unreliable water sources) described observed mosquito and disease dynamics most often, especially in the Kenya sites (Table 2), where household access to piped water is very low (Table 1). The left-skewed unimodal Brière rainfall function (Supplementary Fig. 3a), which indicates that mosquito abundances increase with increasing rainfall until some threshold where flushing occurs, described disease dynamics in some settings, particularly in the Ecuador sites. The symmetric unimodal quadratic rainfall function (Supplementary Fig. 3b), which indicates that mosquito abundances peak with intermediate amounts of rainfall and are reduced with low and high rainfall values, also described disease dynamics in some settings. Interestingly, we did not find a single rainfall function that consistently described dynamics for mosquitoes or arboviral cases across study sites, or for both mosquitoes and arboviral cases within individual study sites (Table 2). In contrast, we did find some consistency with time lags. The model best predicted mosquito abundances in the same month or one month in the future. In more than half of the sites, the model best predicted human disease cases three to four months in the future, and in almost all sites at least two months in the future (the exception is Zaruma, where very few arbovirus cases were reported during the study period and were likely due to importation rather than local

transmission). Given that multiple rainfall functions and time lags are supported by field data (even within the same study site), we propose a conceptual model that incorporates multiple pathways for rainfall to affect disease dynamics along a continuum of rainfall (Fig. 5), in contrast to distinct functional relationships for a given setting, which motivated the approach used in this study.

Factors that mediate disease dynamics predictability

The ability of the model to generate similar dynamics to those found in the field varied with demography, housing quality, and climate. Although the sample size is small (N = 8 sites), we found that the SEI-SEIR model generally predicted vector dynamics better in sites with a smaller proportion of young children in the population ($R^2 = 0.89$, $p < 0.01$; Fig. 6a), lower mean temperature ($R^2 = 0.63$, $p < 0.05$; Fig. 6c), and a larger proportion of homes with piped water ($R^2 = 0.76$, $p < 0.01$; Fig. 6b) and made of cement ($R^2 = 0.69$, $p < 0.05$; Fig. 6d; list of all factors we assessed are provided in Table 1). Based on the range of mean temperatures at our study sites (22 – 28°C), our findings indicate that vector dynamics become less predictable as temperatures near the optimal temperature for transmission (derived in previous studies as 29°C) following the shape and slope in the R_0 curve (Fig. 7). This complements phenomenological models that have found minimal effects of temperature near the empirically derived thermal optima (Fig. 7). None of the socio-economic factors that we examined in this study (Table 1) explained variability in the pairwise correlations for human disease cases among sites.

Discussion:

Directly observing the influence of climate on species interactions and population dynamics is often challenging because of interacting and nonlinear relationships. Here, we directly and quantitatively connect laboratory-based climate relationships to observed mosquito and disease dynamics in the field, supporting the mechanistic role of climate in these disease systems. The trait-based modeling approach captured several key epidemic characteristics and generated a range of disease dynamics along a spectrum of settings with low levels of transmission to seasonal outbreaks, helping to reconcile seemingly context dependent effects (i.e., opposite conclusions about the magnitude and direction of effects; Fig. 7) of climate on arboviral transmission dynamics from the literature [7–12,47].

The results of this study shed some light on the influence of climate in driving endemic versus epidemic dengue transmission. Although Ecuador typically experiences seasonal epidemics [6] and Kenya typically experiences low levels of year-round transmission [5], the sites within this study suggest that epidemic transmission is more common in settings with clear seasonality (e.g., coastal sites) whereas endemic transmission is more common in settings with more climate variability (e.g., inland sites), regardless of country. Coastal sites experienced more regular seasonal climate cycles, likely because oceans buffer climate variability, and this seasonality corresponded with seasonal epidemics. In contrast, the inland sites experienced more day-to-day climate variability, which resulted in more fluctuations in disease cases. As a result, the occurrence and persistence of suitable temperature, rainfall, and humidity conditions enabling outbreaks were less

316 regular in sites with more climate variability. The ability of the model to detect key
317 epidemic characteristics across endemic and epidemic settings indicates that climate
318 plays a major role in driving when outbreaks occur and how long they last.
319
320 Using field data on mosquitoes and disease cases from diverse settings and a model
321 parameterized with data from other studies, we identified several key epidemic
322 characteristics that we should (and should not) expect to capture in new settings. While
323 we would never expect a perfect correlation between model predictions and observations,
324 even if the model perfectly captured climate-host-vector dynamics because of the many
325 additional factors that affect transmission in nature, our results indicate that a model with
326 limited calibration can determine the number of outbreaks across settings remarkably
327 well (Fig. 3a). This finding could be particularly useful for prioritizing surveillance or
328 intervention activities across a range of a potential sites that would otherwise appear
329 equal in their propensity for outbreaks (e.g., similar climate conditions). We also show
330 that the model captures the peak timing of outbreaks (Fig. 3b) and outbreak duration (Fig.
331 3c) but not the final outbreak size (Fig. 3d) or maximum number of infections (Fig. 3e),
332 supporting the hypothesis that the magnitude of disease cases during an outbreak in
333 settings with year-round climate suitability for disease transmission are invariant to
334 temperature, as proposed by [30], likely because the magnitude of disease cases is
335 probably more strongly driven by the availability of susceptible hosts.
336
337 Given that the model generally did not predict the magnitude of outbreaks, we asked how
338 well the model reproduced vector and human disease dynamics (i.e., variation over time)

339 across sites and whether this relationship varied systematically with different socio-
340 economic factors. Across sites, the range of temporal correlations between model
341 predictions and observations (N = 8; Fig. 4, Table 2) provides an informative metric for
342 the proportion of true disease dynamics that we might expect to capture in new settings,
343 ranging from 28 – 88%. The correlations varied with demography, housing construction,
344 and climate (Fig. 6). The model may have better explained vector dynamics in locations
345 with a lower proportion of children under five years old for a variety of reasons,
346 including because bottom-heavy demographic pyramids are often associated with lower
347 socioeconomic status and higher mobility throughout the day. In addition to the
348 demographic makeup of sites, housing construction within sites also seems to modify
349 transmission dynamics: vector dynamics were less predictable in sites with more houses
350 with piped water and made of cement (Fig. 6b,d). These results suggest that piped water
351 may prevent additional contact between humans and mosquitoes associated with stored
352 water around the home. In addition, housing materials like cement that lower indoor
353 temperature could artificially decrease climate suitability for mosquitoes, thereby
354 decreasing the probability that mosquitoes will enter and bite people inside their homes.
355 Despite incorporating all known temperature-dependent mosquito traits into the SEI-
356 SEIR model, we still found vector dynamics became less predictable near the empirically
357 derived thermal optima for arboviral transmission (Figs. 6c, 7). This finding may be
358 associated with physiological or behavioral responses of mosquitoes to temperatures near
359 their thermal safety margin [59,60] and/or humans modifying their environment (as
360 described above) in locations optimal for transmission.
361

Across the study sites, we found support for three hypothesized relationships between rainfall and mosquito carrying capacity as well as several time lags between model predictions and disease observations. Support for multiple rainfall functions could indicate that the effects of rainfall on immature habitat is highly heterogenous, which has been found in previous research in Ecuador [27] and Kenya [61]. Alternatively, the combination of multiple rainfall relationships and time lags could arise from nonlinear and delayed effects of extreme climate such as droughts and floods. More specifically, we hypothesize that there may be multiple mechanistic relationships for the effects of rainfall on mosquito abundance and arboviral disease dynamics (Fig. 5), and they may act on different time scales. For example, previous research indicated that dengue outbreaks were more likely to occur four to five months after a drought and one month after excessive rainfall and a statistical model that incorporated these duel exposure-lag-response functions was highly effective at predicting dengue outbreaks in Barbados [62]. Further, if multiple rainfall relationships act in concert across varying time lags, this would help to explain why many different time lags have been observed between rainfall and arboviral dynamics in previous studies [6,27,51,63–65].

Future research can build on this study to improve our understanding of arboviral dynamics across settings. There were several factors that we did not include in this study, such as existing vector control programs, infrastructure, and preexisting immunity in the population. For instance, in Ecuador, factors such as distance to abandoned properties, interruptions in access to piped water, shaded patios, and use of vector control are documented to influence arbovirus transmission [66], whereas in the study sites in Kenya,

385 factors associated with arboviral transmission are less well studied and there are currently
386 no widely used vector control or local arboviral surveillance programs employed. Future
387 studies could further improve the model by incorporating human immune dynamics
388 associated with interactions among different dengue serotypes [67] or cross-reactivity
389 among viral antibodies [68], differential susceptibility across human age classes [69], and
390 heterogeneity in contact rates between mosquitoes and people based on human behavior
391 and movement [70,71]. Further, as experimental data becomes available for trait
392 estimates specific to chikungunya and Zika, this model could be partitioned to model
393 each arboviral disease individually. This is likely to be an important addition as the
394 different arboviruses tend to peak in different years, possibility due to differences in viral
395 development rates and extrinsic incubation periods among arboviruses. Therefore,
396 validating the model with all three arboviruses combined may oversimplify the complex
397 interannual dynamics that arise due to competition among arboviruses in mosquitoes and
398 humans. There were not enough data for chikungunya and Zika cases in this study to
399 formally test such patterns. This study provides strong evidence that a trait-based model,
400 parameterized independently from field data, can reproduce key epidemic characteristics
401 and a range of spatiotemporal arboviral disease dynamics. Such mechanistic, climate-
402 driven models will become increasingly important to support public health efforts in the
403 face of novel climate regimes emerging due to climate change.
404
405
406
407

Methods:

Climate data

We collected *in situ* measurements of daily mean temperature, relative humidity, and rainfall at each study site and interpolated missing data where necessary. We used temperature and humidity measurements from HOBO loggers and rainfall measurements from rain gauges for sites in Kenya. We used temperature, humidity, and rainfall measurements from automatic weather stations operated by the National Institute of Meteorology and Hydrology in Ecuador. For Kenya, we interpolated missing temperature data from NOAA Global Surface Summary of the Day (Supplementary Table 2, Supplementary Fig. 4) and interpolated missing rainfall data from NOAA Climate Prediction Center Africa Rainfall Climatology dataset (Supplementary Table 2, Supplementary Fig. 5). For Ecuador, we interpolated missing temperature (Supplementary Table 2, Supplementary Fig. 4) and rainfall (Supplementary Table 2, Supplementary Fig. 5) data using the nearest study site where possible and otherwise based on long term mean values for the corresponding Julian day. To interpolate missing data, we linearly regressed all measurements taken on the same day in two datasets and then used the linear model to interpolate temperature for the site with missing data based on the climate measurement from the secondary source for the date when the data was missing (Supplementary Figs. 4-5). For rainfall, we first calculated a moving window of 14-day accumulated rainfall (which is short enough to capture variability and seasonality in rainfall patterns and follows [72]) for each day before interpolation because modeled daily rainfall values are less reliable than accumulated rainfall over a two week period. We interpolated 14-day cumulative rainfall for any day with a missing rainfall value in

the prior 14 days. For both Kenya and Ecuador, we interpolated missing relative humidity data based on long term mean values for the corresponding Julian day (Supplementary Table 2). We then calculated the saturation vapor pressure deficit (SVPD) from temperature and humidity to use in the humidity function because previous research suggests SVPD is a more informative measure of the effect of humidity on mosquito survival compared with relative humidity [73]. To calculate SVPD, we first calculated the saturation vapor pressure as:

$$SVP = 610.7 * 10^{7.5*T/(273.3+T)} \quad (1)$$

where (T) is temperature in degrees Celsius. We then calculated SVPD (in kilopascals) as

$$SVPD = 1 - \frac{RH}{100} * SVP \quad (2)$$

where RH is relative humidity. The final dataset had no missing values for temperature (Supplementary Fig. 6), rainfall (Supplementary Fig. 7), and humidity (Supplementary Fig. 8).

Vector surveys

We collected, counted, sexed, and classified mosquitoes by species, and aggregated the data to mean number of *Aedes aegypti* per house, month, year, and site to account for differences in survey effort across months and sites. We collected adult mosquitoes using Prokopack aspirators [74]. In Ecuador, we collected mosquitoes from approximately 27 houses per site (range = 3-57 houses across four sites) every one-to-two weeks during three, four-month sampling periods between July 2016 and August 2018 (≈ 37 sampling weeks per site) to capture different parts of the transmission season. We aggregated the Ecuador vector data to monthly values (≈ 15 sampling months per site) to correspond

452 with the temporal resolution of surveys in Kenya. In Kenya, we collected mosquitoes
453 from approximately 20 houses per site (range = 1-47 houses across four sites) every
454 month between January 2014 and October 2018 (≈ 54 sampling months per site). In
455 Kenya, we also collected pupae, late instars, and early instars from containers with
456 standing water around the home and collected eggs by setting ovitraps for an average of
457 four days in and around each house monthly. We brought pupae, late and early instars,
458 and eggs to the insectary and reared them to adulthood to classify individuals by sex and
459 species. All mosquito traps capture a small portion of the true mosquito population;
460 therefore, using consistent trapping methods at the same locations through time allows us
461 to compare relative mosquito population dynamics across study sites rather than the
462 absolute magnitude of mosquito abundances.
463
464 Arboviral surveys
465 For Ecuador, we analyzed laboratory-confirmed dengue, chikungunya, and Zika cases
466 provided by the Ministry of Health (MoH) of Ecuador. The MoH collects serum samples
467 from a subset of people with suspected arbovirus infections, and samples are tested at the
468 National Public Health Research Institute by molecular diagnostics (RT-PCR) or
469 antibody tests (IgM ELISA for dengue), depending on the number of days of illness.
470 Results are sent to the MoH Epidemiological Surveillance and Control National
471 Directorate (SIVE Alerta system). Laboratory-confirmed dengue cases were available for
472 all four sites from 2014 to 2018. Laboratory-confirmed chikungunya cases were available
473 for Machala and Huaquillas from 2015 to 2018. Laboratory-confirmed Zika cases were
474 available for Machala from 2016 to 2018.

For Kenya, we used laboratory-confirmed dengue cases aggregated by site and month between 2014 and 2018 collected in a passive surveillance study on childhood febrile illness in Kenya (NIH R01AI102918, PI: ADL). The study population consisted of 7,653 children less than 18 years of age with undifferentiated febrile illness. Children with fever enrolled in the study when attending outpatient care in one of the four study sites (Mbaka Oromo Health Centre in Chulaimbo, Obama Children's Hospital in Kisumu, Msambweni District Hospital in Msambweni, and Ukunda/Diani Health Center in Ukunda). Local health officers collected comprehensive clinical and demographic data and phlebotomy at the initial visit. We tested each child's blood for dengue viremia by molecular diagnostics (conventional PCR [75] or targeted multiplexed real-time PCR when available [76]), or serologic conversion between an initial and a follow up visit (IgG ELISA [77]).

For arboviral data collection in Ecuador and Kenya, participants provided consent and all local and institutional protocols were followed (Stanford IRB #31488, KEMRI ERC #2611).

SEI-SEIR model

We adapted an SEI-SEIR model parameterized for dengue transmission in *Ae. aegypti* mosquitoes [30] to simulate mosquito abundance and arboviral cases through time based on daily weather conditions in eight study locations. The model (equations 3-9; Fig. 2), created independently from the observed data described above, allows mosquito life history traits and viral development rate to vary with temperature (T) following [30],

mosquito carrying capacity to vary with accumulated 14-day rainfall (R) following [72], and mosquito mortality to vary with humidity (i.e., saturation vapor pressure deficit) (H) following [73].

$$\frac{dS_m}{dt} = \varphi(T,H) * \frac{1}{\mu(T,H)} * N_m * \left(1 - \frac{N_m}{K(T,R,H)}\right) - \left(a(T) * pMI(T) * \frac{I_h}{N_h} + \mu(T,H)\right) * S_m \quad (3)$$

$$\frac{dE_m}{dt} = a(T) * pMI(T) * \frac{I_h}{N_h} * S_m - \left(PDR(T) + \mu(T,H)\right) * E_m \quad (4)$$

$$\frac{dI_m}{dt} = PDR(T) * E_m - \mu(T,H) * I_m \quad (5)$$

$$\frac{dS_h}{dt} = -a(T) * b(T) * \frac{I_m}{N_h} * S_h + BR * S_h - DR * S_h + ie * N_h - ie * S_h \quad (6)$$

$$\frac{dE_h}{dt} = a(T) * b(T) * \frac{I_m}{N_h} * S_h - \delta * E_h - DR * E_h - ie * E_h \quad (7)$$

$$\frac{dI_h}{dt} = \delta * E_h - \eta * I_h - DR * I_h - ie * I_h \quad (8)$$

$$\frac{dR_h}{dt} = \eta * I_h - DR * R_h - ie * R_h \quad (9)$$

where

$$\varphi(T,H) = EFD(T) * pEA(T) * MDR(T) \quad (10)$$

The adult mosquito population (N_m) is separated into susceptible (S_m), exposed (E_m), and infectious (I_m) compartments and the human population (N_h) is separated into susceptible (S_h), exposed (E_h), infectious (I_h), and recovered (R_h) compartments (Fig. 2). Climate-independent model parameters include the intrinsic incubation period (δ = 5.9 days), human infectivity period (η =- 5 days), birth rate (BR = 31.782 and 20.175 per 1000 people in Ecuador and Kenya respectively), death rate (DR = 5.284 and 5.121 per 1000 people for Ecuador and Kenya respectively), and immigration/emigration rate (ie = 0.01). The temperature-dependent SEI-SEIR model was developed by Huber et al. [30] and allows mosquito life history traits and viral development rate to vary according to thermal

response curves fit from data derived in laboratory experiments conducted at constant temperatures (Table 3). Although laboratory experiments do not reflect real-world conditions, the physiological responses measured are biologically meaningful. The temperature-dependent traits include eggs laid per female per day (EFD), the probability of egg-to-adult survival (pEA), mosquito development rate (MDR), mosquito mortality rate (lifespan^{-1}; μ), biting rate (a), probability of mosquito infection per bite on an infectious host (pMI), parasite development rate (PDR), and probability of mosquito infectiousness given an infectious bite (b). We modified the mosquito mortality rate equation to vary as a function of temperature and humidity by fitting a spline model based on a pooled survival analysis of *Ae. aegypti* [73] (Supplementary Fig. 9):

$$\mu(T,H) = \frac{1}{c * (T - T_0) * (T - T_m)} + (1 - (0.01 + 2.01 * H)) * y \qquad H < 1 \qquad (11)$$

$$\mu(T,H) = \frac{1}{c * (T - T_0) * (T - T_m)} + (1 - (1.22 + 0.27 * H)) * y \qquad H \geq 1 \qquad (12)$$

where the rate constant (c), minimum temperature (T_0), and maximum temperature (T_m) equal -1.24, 16.63, and 31.85 respectively (Table 3), humidity (H) is the saturation vapor pressure deficit, and y is a scaling factor that we set to 0.005 and 0.01, respectively, to restrict mosquito mortality rates within the range of mortality rates estimated by other studies [19,73]. The linear humidity function has a steeper slope at lower humidity values (equation 11) compared with higher humidity values (equation 12) based on previous research [73] (Supplementary Fig. 9).

We modeled adult mosquito carrying capacity, K, as a modified Arrhenius equation following [30,78]:

$$K(T,H,R) = \frac{EFD(T_0) * pEA(T_0) * MDR(T_0) * \mu(T_0,H_0)^{-1} - \mu(T_0,H_0)}{EFD(T_0) * pEA(T_0) * MDR(T_0) * \mu(T_0,H_0)^{-1}} * N_{m.max} * e^{\frac{-E_A*(T-T_0)^2}{K_B*(T+273)*(T_0+273)}} * f(R) \quad (13)$$

with T_0 and H_0 set to the temperature and humidity where carrying capacity is greatest (i.e., physiological optimal conditions from laboratory experiments; 29°C and 6 kPA), $N_{m.max}$ set to the maximum possible mosquito abundance in a population (twice the human population size following [30]), and the Boltzmann constant, (K_B), is 8.617 x 10^{-5} eV/K. We set the activation energy, E_A, as 0.05 based on [30]. Since there were no experimental data from which to derive the functional response of mosquito carrying capacity across a gradient of rainfall values, we tested several functional relationships based on hypothesized biological relationships between freshwater availability and immature mosquito breeding habitat, modeling the effect of rainfall on carrying capacity, *f*(*R*), as either:

$$f(R_{\text{Brière}}) = c * R * (R - R_{min}) * \sqrt{(R_{max} - R)} * z \quad (14)$$

$$f(R_{Quadratic}) = c * (R - R_{min}) * (R - R_{max}) * z \quad (15)$$

$$f(R_{\text{Inverse}}) = \frac{1}{R} * z \quad (16)$$

where minimum rainfall (R_{min}) equaled 1 mm and maximum rainfall (R_{max}) equaled 123 mm based on the high probability of flushing [26]. The quadratic function is similar to the rainfall function found in [26] and the inverse function is based on the rainfall function used in [72]. We used rate constants (c) of 7.86e^{-5} and -5.99e^{-3} for the Brière and quadratic functions respectively, based on rate constants for other parameters with similar functional forms (Table 3). We also included a scaling factor, z (0. 28, 0.025, and 0.60 respectively), to restrict the maximum carrying capacity to produce model outputs based

550 on a subsample of the total population for comparison with observations. Since the rate
551 constant, c, is multiplied by z, inferring the exact value of c is not necessary because it is
552 scaled by z. The scaling factor could be removed from the model to simulate dynamics in
553 the total population.

554

555 Table 3: Fitted thermal responses for *Ae. aegypti* life history traits. Traits were fit to a
556 Brière $[cT(T-T_0)(T_m-T)^{\frac{1}{2}}]$ or a quadratic $[c(T-T_m)(T-T_0)]$ function where T
557 represents temperature. T_0 and T_m are the critical thermal minimum and maximum,
558 respectively, and c is the rate constant. Thermal responses were fit by [19] and also used
559 in [30]. Parasite development rate was measured as the virus extrinsic incubation rate.

Trait	Definition	Function	c	T_0	T_m
a	Biting rate (day^{-1})	Brière	2.71×10^{-04}	14.67	41.00
EFD	Eggs laid per female per day	Brière	2.08×10^{-02}	14.06	32.03
pEA	Probability of mosquito egg-to-adult survival	Quadratic	-3.36×10^{-03}	7.68	38.31
MDR	Mosquito egg-to-adult development rate (day^{-1})	Brière	1.49×10^{-04}	15.12	37.67
Lf	Adult mosquito lifespan (days)	Quadratic	-1.24	16.63	31.85
b	Probability of mosquito infectiousness	Brière	9.86×10^{-04}	12.05	32.79
pMI	Probability of mosquito infection	Brière	5.23×10^{-04}	1.51	34.74
PDR	Parasite development rate (day^{-1})	Brière	1.04×10^{-04}	11.50	38.97

560

561 To initiate the model, we used site-specific values for human population size and
562 randomly selected one set of values for all sites for the proportion of mosquitoes and
563 humans in each compartment. For Ecuador, we used population estimates from official

564 population projections produced by Proyección de la Población Ecuatoriana, por años
565 calendario, según cantones 2010-2020
566 (https://www.ecuadorencifras.gob.ec/proyecciones-poblacionales/) with population sizes
567 of 57,366, 279,887, 13,673, and 25,615 for Huaquillas, Machala, Portovelo, and Zaruma,
568 respectively, based on 2017 projections. For Kenya, we estimated the population sizes
569 served by each outpatient care facility by creating a polygon around all the geolocations
570 of study participants' homes enrolled at each outpatient care facility and summed
571 population count data from NASA's Socioeconomic Data and Applications Center
572 Gridded Population of the World v4 (https://doi.org/10.7927/H4JW8BX5) within each
573 polygon using ArcGIS v 10.4.1. We estimated population sizes of 7,304, 547,557,
574 240,698, and 154,048 for Chulaimbo, Kisumu, Msambweni, and Ukunda, respectively.
575 We set the ratio of mosquitoes to humans to two, following [30]. We used the following
576 values as the initial proportion of mosquitoes and humans in each model compartment:
577 S_m = 0.22, E_m = 0.29, I_m = 0.49, S_h = 0.58, E_h = 0.22, I_h = 0.00, and R_h = 0.20. We
578 determined that the model was invariant to initial proportion values after a short burn-in
579 period (90 days) based on a sensitivity analysis (Supplementary Fig. 10); therefore, we
580 randomly selected one set of initial proportion values from the sensitivity analysis for all
581 the model simulations. We also determined that the temporal trajectories of model
582 dynamics did not change when we varied the critical thermal minimum, maximum, and
583 rate constants (Table 3) for *Aedes aegypti* life history traits (Supplementary Figs. 1-2).
584
585 We ran all model simulations using the deSolve package in R statistical software v 3.5.3
586 [79].

587

588 Model validation

589 To validate the SEI-SEIR model, we calculated pairwise correlations with an adjusted p-
590 value to account for autocorrelation for each site. For the pairwise correlations, we used
591 the ccf function in base R [79] to calculate correlations between the two times series of
592 model predictions and observations with 0, 1, 2, 3, 4, and 5-month lags. We then
593 calculated an adjusted p-value using the Modified Chelton method [45] to adjust the null
594 hypothesis test of sample correlation between autocorrelated time series. To assess
595 predictions and observations for vector dynamics for each site, we compared monthly
596 time series of the total predicted mosquito population from the SEI-SEIR model with the
597 monthly time series of mean number of *Aedes aegypti* (per house). We followed the same
598 procedure to compare model predictions with other mosquito life stages for sites in
599 Kenya. Similarly, to compare predictions and observations for human disease dynamics
600 for each site, we compared monthly times series of predicted infected individuals from
601 the SEI-SEIR model with the monthly time series of total laboratory-confirmed arboviral
602 cases. For subsequent analyses, we used model predictions from the model (e.g., SEI-
603 SEIR model with a specific rainfall function and time lag) with the highest pairwise
604 correlation value.

605

606 To compare key epidemic characteristics between model predictions and observations
607 and to compare site-specific correlations with socio-economic factors, we used linear
608 regression models using the lm function in that stats package in R [79]. We defined
609 outbreaks as a continuous time period where the peak cases exceeded the mean number

610 of cases (predicted or observed) plus one standard deviation within a site. We then used
611 those outbreak periods to count the total number of outbreaks within each site, and, for
612 predicted and observed outbreaks that overlapped in time, the duration, peak timing total
613 outbreak size, and maximum number of infections. We compared predictions and
614 observations for each of these metrics with linear regression. Since we were interested in
615 whether model predictions matched observations for each independent outbreak period,
616 we did not allow varying intercepts or slopes by site. Similarly, we compared the
617 pairwise correlation values (described above) across all sites with each socio-economic
618 factor listed in Table 1 separately using linear regressions.
619
620 Comparison of R_0 with prior studies
621 We collected effect sizes of temperature on dengue incidence from 12 peer-reviewed
622 studies from the literature (Supplementary Table 1). We selected studies with mean
623 temperatures across the predicted temperature range where arboviral transmission can
624 occur. We scaled the coefficient values to visualize the relative effect of temperature
625 across studies given that the original analyses were conducted with different temperature
626 metrics and across different temperature ranges. We provide additional information and
627 sources in Supplementary Table 1.
628
629 Data Availability statement
630 All data that support the findings of this study are deposited in a public repository, with
631 the exception of arboviral incidence data from Ecuador, which is available from the
632 corresponding author upon reasonable request. Climate, epidemic characteristics, socio-

economic, vector, and Kenya arboviral incidence data that we analyzed in this study are available in the following public repository: https://github.com/jms5151/SEI-SEIR_Arboviruses. This data supported Figures 3, 4, and 6 in the main text and Supplemental Figures 1-3 and 6-10. Data that supports Figure 7 is available in Supplemental Table 1. The arboviral case data from Ecuador are available from the corresponding author upon reasonable request. The data are not publicly available due to a Confidentiality Agreement with the Ecuador Ministry of Health. Crude birth and death rates used in the model are from The World Bank Open Data. The URL for crude birth rate in Ecuador is https://data.worldbank.org/indicator/SP.DYN.CBRT.IN?locations=EC and for Kenya is https://data.worldbank.org/indicator/SP.DYN.CBRT.IN?locations=KE. The URL for crude death rate for Ecuador is https://data.worldbank.org/indicator/SP.DYN.CDRT.IN?locations=EC and for Kenya is https://data.worldbank.org/indicator/SP.DYN.CDRT.IN?locations=KE.

Code availability

Model and analysis codes are available at https://github.com/jms5151/SEI-SEIR_Arboviruses.

Acknowledgements

JMC, ADL, EFL, and EAM were supported by a Stanford Woods Institute for the Environment – Environmental Ventures Program grant (PIs: EAM, ADL, and EFL). EAM was also supported by a Hellman Faculty Fellowship and a Terman Award. ADL,

656 BAN, FMM, ENGS, MSS, ARK, RD, AA, and HNN were supported by a National
657 Institutes of Health R01 grant (AI102918; PI: ADL). EAM, AMSI, and SJR were
658 supported by a National Science Foundation (NSF) Ecology and Evolution of Infectious
659 Diseases (EEID) grant (DEB-1518681) and AMSI and SJR were also supported by an
660 NSF DEB RAPID grant (1641145). EAM was also supported by a National Institute of
661 General Medical Sciences Maximizing Investigators' Research Award grant
662 (R35GM133439) and an NSF and Fogarty International Center EEID grant (DEB-
663 2011147). We thank Cat Lippi for assistance with formatting household quality survey
664 data from Ecuador.

665

666 Author contributions

667 EAM, ADL, EFL, and JMC conceived of project. JMC conducted analyses and wrote
668 manuscript. EAM, ADL, EFL, and AMSI secured funding for the project. BNN, FMM,
669 EBA, AA, MJBC, RD, FHH, RM, and HNN collected data. ENGS and MMS conducted
670 laboratory analyses. ARK, SJR, and RS processed data. All authors revised and approved
671 of the manuscript.

672

673 Competing Interests

674 The authors declare no competing interests.

675

676 Figure 1: Study sites within two equatorial countries: (a) Ecuador in South America and
677 (b) Kenya in East Africa. We created this map in R using Google Maps as the base layer.

678

679 Figure 2: SEI-SEIR epidemiological model framework. The mosquito population is split
680 among susceptible (S_m), exposed (E_m), and infectious (I_m) compartments (squares) and
681 the human population is split among susceptible (S_h), exposed (E_h), infectious (I_h), and
682 recovered (R_h) compartments. Solid arrows indicate the direction individuals can move
683 between classes and dashed arrows indicate the direction of transmission. Transitions
684 among compartments are labeled by the appropriate processes and corresponding rate
685 parameters (see Methods for parameter definitions and more detail). Rate parameters with
686 a T, H, and R are temperature-, humidity-, and rainfall-dependent, respectively. The total
687 adult mosquito population (S_m, E_m, and I_m compartments; dotted rectangle) is maintained
688 at an abundance less than or equal to the mosquito carrying capacity.
689
690 Figure 3: Model predictions for the number, timing, and duration of arboviral outbreaks
691 closely matched field observations. Scatterplots show model predictions versus
692 observations for different epidemic characteristics. (a) Number of outbreaks indicates the
693 total number of predicted and observed outbreaks in a site over the study period. (b)
694 Timing of outbreak peak, (c) outbreak duration, (d) outbreak size, and (e) maximum
695 infections (e.g., max I_h during an outbreak) correspond to individual outbreaks where
696 model predictions and observations overlapped in time, therefore, some plots show
697 multiple data points per site. Outbreaks are colored by site with different symbols for
698 Ecuador (circles) and Kenya (triangles). We show regression lines and associated
699 statistics (R^2 = coefficient of determination; p-value = probability of two-sided
700 hypothesis test) for statistically significant relationships. For visualization purposes, we
701 jittered the data points to show overlapping data and we excluded data from Machala in

plots (d) outbreak size and (e) maximum infections because the magnitude differed substantially from all other sites.

Figure 4: Model predicts vector and human disease dynamics better in some settings than others. Each plot shows the time series of SEI-SEIR model predictions (grey dots connected by grey lines) and field observations (black dots connected by black lines) for vector (top two rows) and human disease (bottom two rows) dynamics for each study site with the pairwise correlation (r) and adjusted p-value for two-sided hypothesis test (p). We calculated observed mosquito abundances as the mean number of adult *Ae. aegypti* per house, month, year, and site. We calculated observed arboviral cases as the total number of laboratory-confirmed dengue (any serotype), chikungunya, and Zika cases per month, year, and site; six of the eight study sites only included dengue cases (see Methods). The first and third rows show sites in Ecuador and the second and fourth rows show sites in Kenya. We show uncertainty in model predictions in Supplementary Figs. 1-2.

Figure 5: Conceptual model for nonlinear functional relationships between rainfall and vector abundance and arboviral outbreak risk. Dashed lines show multiple potential pathways for rainfall to affect transmission dynamics and include the functional relationships supported in this study. Labels indicate the hypothesized mechanisms along a gradient of rainfall. Adapted from the following source: [46].

Figure 6: Demography, housing construction, and climate affect model predictive capacity for vectors. Factors that influence the predictability of vector dynamics include (a) proportion of the population under five years of age, (b) proportion of houses with piped water, (c) mean temperature, and (d) proportion of houses made with cement (walls and/or floors). Points indicate the pairwise correlation value for a single site (colors) with different symbols for Ecuador (circles) and Kenya (triangles). Each plot also shows the linear regression lines and associated statistics (R^2 = coefficient of determination; p-value = probability of two-sided hypothesis test).

Figure 7: Independently predicted relative R_0 from a model derived from laboratory studies explains differences in the magnitude and direction of the effects of temperature on dengue transmission in the field across varied settings from previous studies. The black line shows the relative basic reproductive number (R_0, normalized to a 0-1 scale) plotted against temperature based on all temperature-dependent traits from [19] used in the SEI-SEIR model presented here. Points indicate mean temperature values from previous field-based statistical analyses that related dengue cases with minimum, maximum, or mean ambient temperature; arrows correspond to the direction (up = positive, down = negative) and relative effect size of the temperature – dengue relationship based on coefficient values from the following studies: [47,48,57,58,49–56]. See Methods and Supplementary Table 1 for more detail. As expected, the largest observed positive effects of temperature occurred in the rapidly increasing portion of the R_0 curve (~22-25°C; consistent with findings in this study) and the largest observed

746 negative effects occurred well above the predicted optimum, near the upper thermal limit
747 (~33-35°C).
748
749
750 References

751 1. Ockendon N, Baker DJ, Carr JA, White EC, Almond REA, Amano T, et al.
752 Mechanisms underpinning climatic impacts on natural populations: altered species
753 interactions are more important than direct effects. Glob Chang Biol. 2014;20:
754 2221–2229. doi:10.1111/gcb.12559
755 2. Boggs CL, Inouye DW. A single climate driver has direct and indirect effects on
756 insect population dynamics. Ecol Lett. 2012;15: 502–508. doi:10.1111/j.1461-
757 0248.2012.01766.x
758 3. Burkett VR, Wilcox DA, Stottlemyer R, Barrow W, Fagre D, Baron J, et al.
759 Nonlinear dynamics in ecosystem response to climatic change: Case studies and
760 policy implications. Ecol Complex. 2005;2: 357–394.
761 doi:10.1016/j.ecocom.2005.04.010
762 4. Molnár PK, Sckrabulis JP, Altman KA, Raffel TR. Thermal Performance Curves
763 and the Metabolic Theory of Ecology—A Practical Guide to Models and
764 Experiments for Parasitologists. J Parasitol. 2017;103. doi:10.1645/16-148
765 5. Hortion J, Mutuku FM, Eyherabide AL, Vu DM, Boothroyd DB, Grossi-Soyster
766 EN, et al. Acute Flavivirus and Alphavirus Infections among Children in Two
767 Different Areas of Kenya, 2015. Am J Trop Med Hyg. 2019;100: 170–173.
768 doi:10.4269/ajtmh.18-0297

6. Stewart-Ibarra AM, Lowe R. Climate and Non-Climate Drivers of Dengue Epidemics in Southern Coastal Ecuador. Am J Trop Med Hyg. 2013;88: 971–981. doi:10.4269/ajtmh.12-0478

7. Jury MR. Climate influence on dengue epidemics in Puerto Rico. Int J Environ Health Res. 2008;18: 323–334. doi:10.1080/09603120701849836

8. Campbell KM, Haldeman K, Lehnig C, Munayco C V., Halsey ES, Laguna-Torres VA, et al. Weather Regulates Location, Timing, and Intensity of Dengue Virus Transmission between Humans and Mosquitoes. Michael E, editor. PLoS Negl Trop Dis. 2015;9: e0003957. doi:10.1371/journal.pntd.0003957

9. Adde A, Roucou P, Mangeas M, Ardillon V, Desenclos J-C, Rousset D, et al. Predicting Dengue Fever Outbreaks in French Guiana Using Climate Indicators. Scarpino S V., editor. PLoS Negl Trop Dis. 2016;10: e0004681. doi:10.1371/journal.pntd.0004681

10. Dhimal M, Gautam I, Joshi HD, O'Hara RB, Ahrens B, Kuch U, et al. Risk Factors for the Presence of Chikungunya and Dengue Vectors (Aedes aegypti and Aedes albopictus), Their Altitudinal Distribution and Climatic Determinants of Their Abundance in Central Nepal. Turell MJ, editor. PLoS Negl Trop Dis. 2015;9: e0003545. doi:10.1371/journal.pntd.0003545

11. Descloux E, Mangeas M, Menkes CE, Lengaigne M, Leroy A, Tehei T, et al. Climate-Based Models for Understanding and Forecasting Dengue Epidemics. Anyamba A, editor. PLoS Negl Trop Dis. 2012;6: e1470. doi:10.1371/journal.pntd.0001470

12. Aswi A, Cramb SM, Moraga P, Mengersen K. Epidemiology and Infection

Bayesian spatial and spatio-temporal approaches to modelling dengue fever: a systematic review. Epidemiol Infect. 2018;147. doi:10.1017/S0950268818002807

13. Johansson MA, Apfeldorf KM, Dobson S, Devita J, Buczak AL, Baugher B, et al. An open challenge to advance probabilistic forecasting for dengue epidemics. Proc Natl Acad Sci. 2019; 201909865. doi:10.1073/pnas.1909865116

14. Michael E, Singh BK, Mayala BK, Smith ME, Hampton S, Nabrzyski J. Continental-scale, data-driven predictive assessment of eliminating the vector-borne disease, lymphatic filariasis, in sub-Saharan Africa by 2020. BMC Med. 2017;15: 176. doi:10.1186/s12916-017-0933-2

15. Smith T, Maire N, Ross A, Penny M, Chitnis N, Schapira A, et al. Towards a comprehensive simulation model of malaria epidemiology and control. Parasitology. 2008. pp. 1507–1516. doi:10.1017/S0031182008000371

16. Ryan SJ, Carlson CJ, Mordecai EA, Johnson LR. Global expansion and redistribution of Aedes-borne virus transmission risk with climate change. Han BA, editor. PLoS Negl Trop Dis. 2019;13: e0007213. doi:10.1371/journal.pntd.0007213

17. Kraemer MU, Sinka ME, Duda KA, Mylne AQ, Shearer FM, Barker CM, et al. The global distribution of the arbovirus vectors *Aedes aegypti* and *Ae. albopictus*. Elife. 2015;4. doi:10.7554/eLife.08347

18. Powell JR, Tabachnick WJ, Powell JR, Tabachnick WJ. History of domestication and spread of Aedes aegypti - A Review. Mem Inst Oswaldo Cruz. 2013;108: 11–17. doi:10.1590/0074-0276130395

19. Mordecai EA, Cohen JM, Evans M V., Gudapati P, Johnson LR, Lippi CA, et al.

Detecting the impact of temperature on transmission of Zika, dengue, and chikungunya using mechanistic models. Althouse B, editor. PLoS Negl Trop Dis. 2017;11: e0005568. doi:10.1371/journal.pntd.0005568

20. Shocket MS, Ryan SJ, Mordecai EA. Temperature explains broad patterns of Ross River virus transmission. Elife. 2018; doi:10.7554/eLife.37762.001

21. Paull SH, Horton DE, Ashfaq M, Rastogi D, Kramer LD, Diffenbaugh NS, et al. Drought and immunity determine the intensity of West Nile virus epidemics and climate change impacts. Proc R Soc B Biol Sci. 2017;284: 20162078. doi:10.1098/rspb.2016.2078

22. Costa EAP de A, Santos EM de M, Correia JC, Albuquerque CMR de. Impact of small variations in temperature and humidity on the reproductive activity and survival of Aedes aegypti (Diptera, Culicidae). Rev Bras Entomol. 2010;54: 488–493. doi:10.1590/S0085-56262010000300021

23. Gaaboub IA, El-Sawaf SK, El-Latif MA. Effect of Different Relative Humidities and Temperatures on Egg-Production and Longevity of Adults of Anopheles (Myzomyia) pharoensis Theob.1. Zeitschrift für Angew Entomol. 2009;67: 88–94. doi:10.1111/j.1439-0418.1971.tb02098.x

24. Koenraadt CJM, Harrington LC. Flushing Effect of Rain on Container-Inhabiting Mosquitoes Aedes aegypti and Culex pipiens (Diptera: Culicidae). J Med Entomol. 2009;45: 28–35. doi:10.1603/0022-2585(2008)45[28:FEOROC]2.0.CO;2

25. Paaijmans KP, Wandago MO, Githeko AK, Takken W, Vulule J. Unexpected High Losses of Anopheles gambiae Larvae Due to Rainfall. Carter D, editor. PLoS One. 2007;2: e1146. doi:10.1371/journal.pone.0001146

838 26. Benedum CM, Seidahmed OME, Eltahir EAB, Markuzon N. Statistical modeling
839 of the effect of rainfall flushing on dengue transmission in Singapore. Reiner RC,
840 editor. PLoS Negl Trop Dis. 2018;12: e0006935.
841 doi:10.1371/journal.pntd.0006935
842 27. Stewart Ibarra AM, Ryan SJ, Beltrán E, Mejía R, Silva M, Muñoz Á. Dengue
843 Vector Dynamics (Aedes aegypti) Influenced by Climate and Social Factors in
844 Ecuador: Implications for Targeted Control. Mores CN, editor. PLoS One. 2013;8:
845 e78263. doi:10.1371/journal.pone.0078263
846 28. Pontes RJ, Spielman A, Oliveira-Lima JW, Hodgson JC, Freeman J. Vector
847 densities that potentiate dengue outbreaks in a Brazilian city. Am J Trop Med Hyg.
848 2000;62: 378–383. doi:10.4269/ajtmh.2000.62.378
849 29. Anyamba A, Linthicum KJ, Small JL, Collins KM, Tucker CJ, Pak EW, et al.
850 Climate Teleconnections and Recent Patterns of Human and Animal Disease
851 Outbreaks. Zhou X-N, editor. PLoS Negl Trop Dis. 2012;6: e1465.
852 doi:10.1371/journal.pntd.0001465
853 30. Huber JH, Childs ML, Caldwell JM, Mordecai EA. Seasonal temperature variation
854 influences climate suitability for dengue, chikungunya, and Zika transmission.
855 Althouse B, editor. PLoS Negl Trop Dis. 2018;12: e0006451.
856 doi:10.1371/journal.pntd.0006451
857 31. Lourenço J, Recker M. The 2012 Madeira Dengue Outbreak: Epidemiological
858 Determinants and Future Epidemic Potential. Scarpino S V., editor. PLoS Negl
859 Trop Dis. 2014;8: e3083. doi:10.1371/journal.pntd.0003083
860 32. Li R, Xu L, Bjørnstad ON, Liu K, Song T, Chen A, et al. Climate-driven variation

in mosquito density predicts the spatiotemporal dynamics of dengue. Proc Natl Acad Sci. 2019;119: 3624–3629. doi:10.1073/PNAS.1806094116

33. Wang X, Tang S, Cheke RA. A stage structured mosquito model incorporating effects of precipitation and daily temperature fluctuations. J Theor Biol. 2016;411: 27–36. doi:10.1016/j.jtbi.2016.09.015

34. Siraj AS, Oidtman RJ, Huber JH, Kraemer MUG, Brady OJ, Johansson MA, et al. Temperature modulates dengue virus epidemic growth rates through its effects on reproduction numbers and generation intervals. Althouse B, editor. PLoS Negl Trop Dis. 2017;11: e0005797. doi:10.1371/journal.pntd.0005797

35. Oidtman RJ, Lai S, Huang Z, Yang J, Siraj AS, Reiner RC, et al. Inter-annual variation in seasonal dengue epidemics driven by multiple interacting factors in Guangzhou, China. Nat Commun. 2019;10. doi:10.1038/s41467-019-09035-x

36. Stewart-Ibarra AM, Muñoz ÁG, Ryan SJ, Ayala EB, Borbor-Cordova MJ, Finkelstein JL, et al. Spatiotemporal clustering, climate periodicity, and social-ecological risk factors for dengue during an outbreak in Machala, Ecuador, in 2010. BMC Infect Dis. 2014;14: 610. doi:10.1186/s12879-014-0610-4

37. Agha SB, Tchouassi DP, Turell MJ, Bastos ADS, Sang R. Entomological assessment of dengue virus transmission risk in three urban areas of Kenya. Reiner RC, editor. PLoS Negl Trop Dis. 2019;13: e0007686. doi:10.1371/journal.pntd.0007686

38. Agha SB, Tchouassi DP, Bastos ADS, Sang R. Dengue and yellow fever virus vectors: seasonal abundance, diversity and resting preferences in three Kenyan cities. Parasit Vectors. 2017;10: 628. doi:10.1186/s13071-017-2598-2

884 39. Chretien J-P, Anyamba A, Bedno SA, Breiman RF, Sang R, Sergon K, et al.
885 Drought-Associated Chikungunya Emergence Along Coastal East Africa. Am J
886 Trop Med Hyg. 2007;76: 405–407. doi:10.4269/ajtmh.2007.76.405
887 40. Vu DM, Mutai N, Heath CJ, Vulule JM, Mutuku FM, Ndenga BA, et al.
888 Unrecognized Dengue Virus Infections in Children, Western Kenya, 2014-2015.
889 Emerg Infect Dis. 2017;23: 1915–1917. doi:10.3201/eid2311.170807
890 41. Gubler DJ, Nalim S, Saroso JS, Saipan H, Tan R. Variation in Susceptibility to
891 Oral Infection with Dengue Viruses among Geographic Strains of Aedes Aegypti
892 *. Am J Trop Med Hyg. 1979;28: 1045–1052. doi:10.4269/ajtmh.1979.28.1045
893 42. Xavier-Carvalho C, Chester Cardoso C, de Souza Kehdya F, Guilherme Pacheco
894 A, Ozório Moraesa M. Host genetics and dengue fever. Infect Genet Evol.
895 2017;56: 99–110. doi:10.1016/J.MEEGID.2017.11.009
896 43. Didan K, Barreto Munoz A, Solano R, Huete A. MODIS Vegetation Index User's
897 Guide (MOD13 Series) [Internet]. Available: http://vip.arizona.edu
898 44. Sulla-Menashe D, Friedl MA. User Guide to Collection 6 MODIS Land Cover
899 (MCD12Q1 and MCD12C1) Product. 2018; doi:10.5067/MODIS/MCD12Q1
900 45. Pyper BJ, Peterman RM. Comparison of methods to account for autocorrelation in
901 correlation analyses of fish data. Can J Fish Aquat Sci. 1998;55: 2127–2140.
902 doi:10.1139/f98-104
903 46. Shocket MS, Anderson CB, Caldwell JM, Childs ML, Han S, Harris M, et al.
904 Environmental drivers of vector-borne disease. Population Biology of Vector-
905 borne Diseases. Oxford University Press;
906 47. Hurtado-Daz M, Riojas-Rodrguez H, Rothenberg S, Gomez-Dantes H, Cifuentes

907 E. Impact of climate variability on the incidence of dengue in Mexico. Trop Med
908 Int Heal. 2007;12. doi:10.1111/j.1365-3156.2007.01930.x
909 48. Colón-González FJ, Bentham G, Lake IR. Climate Variability and Dengue Fever
910 in Warm and Humid Mexico. Am J Trop Med Hyg. 2011;84: 757–763.
911 doi:10.4269/ajtmh.2011.10-0609
912 49. Wang C, Jiang B, Fan J, Wang F, Liu Q. A Study of the Dengue Epidemic and
913 Meteorological Factors in Guangzhou, China, by Using a Zero-Inflated Poisson
914 Regression Model. Asia Pacific J Public Heal. 2014;26: 48–57.
915 doi:10.1177/1010539513490195
916 50. Minh An DT, Rocklöv J. Epidemiology of dengue fever in Hanoi from 2002 to
917 2010 and its meteorological determinants. Glob Health Action. 2014;7: 23074.
918 doi:10.3402/gha.v7.23074
919 51. Laureano-Rosario AE, Garcia-Rejon JE, Gomez-Carro S, Farfan-Ale JA, Muller-
920 Kargera FE. Modelling dengue fever risk in the State of Yucatan, Mexico using
921 regional-scale satellite-derived sea surface temperature. Acta Trop. 2017;172: 50–
922 57. doi:10.1016/j.actatropica.2017.04.017
923 52. Wu P-C, Guoa H-R, Lung S-C, Lin C-Y, Su H-J. Weather as an effective predictor
924 for occurrence of dengue fever in Taiwan. Acta Trop. 2007;103: 50–57.
925 doi:10.1016/j.actatropica.2007.05.014
926 53. Karim MN, Munshi SU, Anwar N, Alam MS. Climatic factors influencing dengue
927 cases in Dhaka city: a model for dengue prediction. Indian J Med Res. 2012;136:
928 32–9. Available: http://www.ncbi.nlm.nih.gov/pubmed/22885261
929 54. Nakhapakorn K, Tripathi N. An information value based analysis of physical and

climatic factors affecting dengue fever and dengue haemorrhagic fever incidence. Int J Health Geogr. 2005;4: 13. doi:10.1186/1476-072X-4-13

55. Gharbi M, Quenel P, Gustave J, Cassadou S, Ruche G La, Girdary L, et al. Time series analysis of dengue incidence in Guadeloupe, French West Indies: Forecasting models using climate variables as predictors. BMC Infect Dis. 2011;11: 166. doi:10.1186/1471-2334-11-166

56. Sharmin S, Glass K, Viennet E, Harley D. Interaction of Mean Temperature and Daily Fluctuation Influences Dengue Incidence in Dhaka, Bangladesh. Kasper M, editor. PLoS Negl Trop Dis. 2015;9: e0003901. doi:10.1371/journal.pntd.0003901

57. Sriprom M, Chalvet-Monfray K, Chaimane T, Vongsawat K, Bicout DJ. Monthly district level risk of dengue occurrences in Sakon Nakhon Province, Thailand. Sci Total Environ. 2010;408: 5521–5528. doi:10.1016/J.SCITOTENV.2010.08.024

58. Martínez-Bello D, López-Quílez A, Prieto AT. Spatiotemporal modeling of relative risk of dengue disease in Colombia. Stoch Environ Res Risk Assess. 2018;32: 1587–1601. doi:10.1007/s00477-017-1461-5

59. Mordecai EA, Caldwell JM, Grossman MK, Lippi CA, Johnson LR, Neira M, et al. Thermal biology of mosquito-borne disease. Byers J (Jeb), editor. Ecol Lett. 2019; ele.13335. doi:10.1111/ele.13335

60. Carrington LB, Armijos MV, Lambrechts L, Barker CM, Scott TW. Effects of Fluctuating Daily Temperatures at Critical Thermal Extremes on Aedes aegypti Life-History Traits. PLoS One. 2013;8. doi:10.1371/journal.pone.0058824

61. Ngugi HN, Mutuku FM, Ndenga BA, Musunzaji PS, Mbakaya JO, Aswani P, et al. Characterization and productivity profiles of Aedes aegypti (L.) breeding habitats

across rural and urban landscapes in western and coastal Kenya. Parasit Vectors. 2017;10: 331. doi:10.1186/s13071-017-2271-9

62. Lowe R, Gasparrini A, Van Meerbeeck CJ, Lippi CA, Mahon R, Trotman AR, et al. Nonlinear and delayed impacts of climate on dengue risk in Barbados: A modelling study. PLoS Med. 2018;15. doi:10.1371/journal.pmed.1002613

63. Li C, Wang X, Wu X, Liu J, Ji D, Du J. Modeling and projection of dengue fever cases in Guangzhou based on variation of weather factors. Sci Total Environ. 2017;605–606: 867–873. doi:10.1016/j.scitotenv.2017.06.181

64. Li CF, Lim TW, Han LL, Fang R. Rainfall, abundance of Aedes aegypti and dengue infection in Selangor, Malaysia. Southeast Asian J Trop Med Public Health. 1985;16: 560–8. Available: http://www.ncbi.nlm.nih.gov/pubmed/3835698

65. Johansson MA, Dominici F, Glass GE. Local and Global Effects of Climate on Dengue Transmission in Puerto Rico. Massad E, editor. PLoS Negl Trop Dis. 2009;3: e382. doi:10.1371/journal.pntd.0000382

66. Kenneson A, Beltrán-Ayala E, Borbor-Cordova MJ, Polhemus ME, Ryan SJ, Endy TP, et al. Social-ecological factors and preventive actions decrease the risk of dengue infection at the household-level: Results from a prospective dengue surveillance study in Machala, Ecuador. Messer WB, editor. PLoS Negl Trop Dis. 2017;11: e0006150. doi:10.1371/journal.pntd.0006150

67. Reich NG, Shrestha S, King AA, Rohani P, Lessler J, Kalayanarooj S, et al. Interactions between serotypes of dengue highlight epidemiological impact of cross-immunity. J R Soc Interface. 2013;10: 20130414. doi:10.1098/rsif.2013.0414

68. Wen J, Elong Ngono A, Regla-Nava JA, Kim K, Gorman MJ, Diamond MS, et al. Dengue virus-reactive CD8+ T cells mediate cross-protection against subsequent Zika virus challenge. Nat Commun. 2017;8: 1459. doi:10.1038/s41467-017-01669-z

69. Rodriguez-Barraquer I, Salje H, Cummings DA. Opportunities for improved surveillance and control of dengue from age-specific case data. Elife. 2019;8. doi:10.7554/eLife.45474

70. Stoddard ST, Forshey BM, Morrison AC, Paz-Soldan VA, Vazquez-Prokopec GM, Astete H, et al. House-to-house human movement drives dengue virus transmission. Proc Natl Acad Sci U S A. 2013;110: 994–999. doi:10.1073/pnas.1213349110

71. Wesolowski A, Qureshi T, Boni MF, Sundsøy PR, Johansson MA, Rasheed SB, et al. Impact of human mobility on the emergence of dengue epidemics in Pakistan. Proc Natl Acad Sci. 2015;112: 11887–11892. doi:10.1073/pnas.1504964112

72. Vaidya A, Bravo-Salgado AD, Mikler AR. Modeling climate-dependent population dynamics of mosquitoes to guide public health policies. Proc 5th ACM Conf Bioinformatics, Comput Biol Heal Informatics - BCB '14. 2014; 380–389. doi:10.1145/2649387.2649415

73. Schmidt CA, Comeau G, Monaghan AJ, Williamson DJ, Ernst KC. Effects of desiccation stress on adult female longevity in Aedes aegypti and Ae. albopictus (Diptera: Culicidae): results of a systematic review and pooled survival analysis. Parasit Vectors. 2018;11: 267. doi:10.1186/s13071-018-2808-6

74. Vazquez-Prokopec GM, Galvin WA, Kelly R, Kitron U. A New, Cost-Effective,

Battery-Powered Aspirator for Adult Mosquito Collections. J Med Entomol. 2009;46: 1256–1259. doi:10.1603/033.046.0602

75. Waggoner JJ, Gresh L, Mohamed-Hadley A, Ballesteros G, Davila MJV, Tellez Y, et al. Single-Reaction Multiplex Reverse Transcription PCR for Detection of Zika, Chikungunya, and Dengue Viruses. Emerg Infect Dis. 2016;22: 1295–7. doi:10.3201/eid2207.160326

76. Lanciotti RS, Calisher CH, Gubler DJ, Chang GJ, Vorndam A V. Rapid detection and typing of dengue viruses from clinical samples by using reverse transcriptase-polymerase chain reaction. J Clin Microbiol. 1992;30: 545–51. Available: http://www.ncbi.nlm.nih.gov/pubmed/1372617

77. Grossi-Soyster EN, Cook EAJ, de Glanville WA, Thomas LF, Krystosik AR, Lee J, et al. Serological and spatial analysis of alphavirus and flavivirus prevalence and risk factors in a rural community in western Kenya. Bingham A, editor. PLoS Negl Trop Dis. 2017;11: e0005998. doi:10.1371/journal.pntd.0005998

78. Palamara GM, Childs DZ, Clements CF, Petchey OL, Plebani M, Smith MJ. Inferring the temperature dependence of population parameters: The effects of experimental design and inference algorithm. Ecol Evol. 2014;4: 4736–4750. doi:10.1002/ece3.1309

79. Team RC. R: A Language and Environment for Statistical Computing. R Found Stat Comput. 2018; Available: https://www.r-project.org

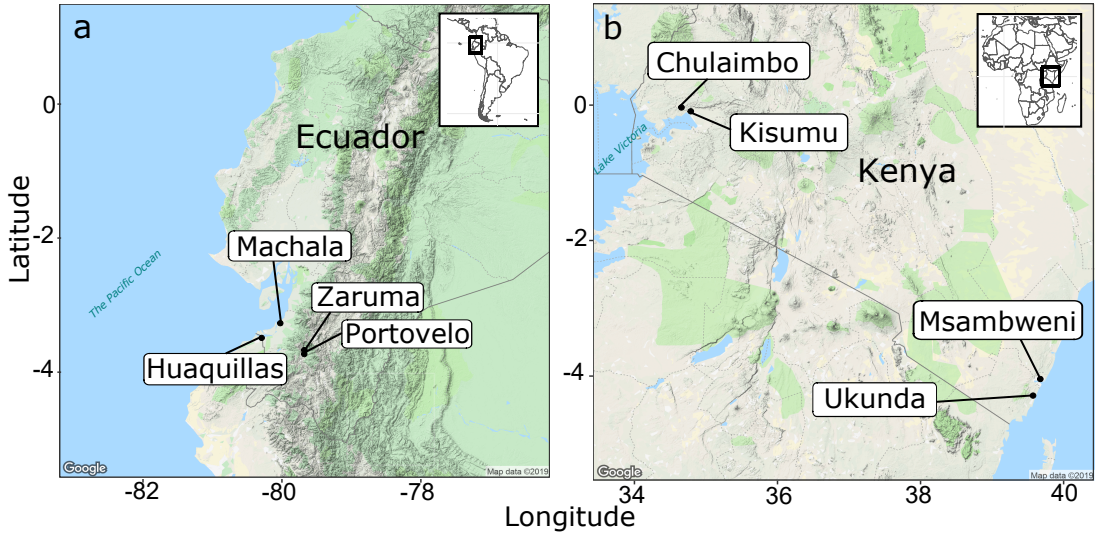
a
Ecuador
Machala
Zaruma
Portovelo
Huaquillas
The Pacific Ocean
Google
Map data ©2019
b
Chulaimbo
Kisumu
Lake Victoria
Kenya
Msambweni
Ukunda
Google
Map data ©2019
Latitude
0
-2
-4
Longitude
-82
-80
-78
34
36
38
40

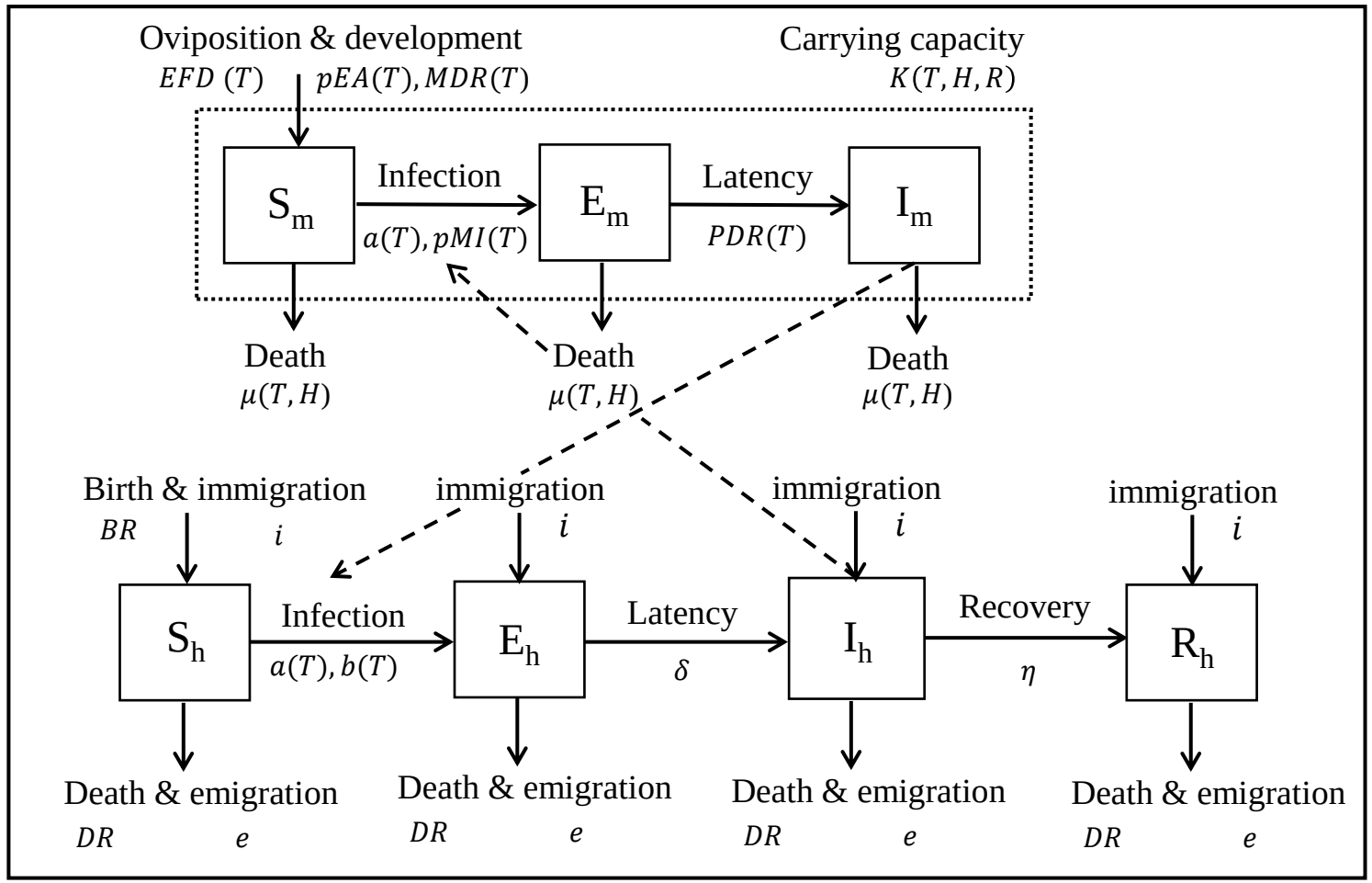
Oviposition & development
$EFD\ (T)$
$pEA(T), MDR(T)$
Carrying capacity
$K(T, H, R)$
S_m
Infection
$a(T), pMI(T)$
E_m
Latency
$PDR(T)$
I_m
Death
$\mu(T, H)$
Death
$\mu(T, H)$
Death
$\mu(T, H)$
Birth & immigration
BR
i
immigration
i
immigration
i
immigration
i
S_h
Infection
$a(T), b(T)$
E_h
Latency
δ
I_h
Recovery
η
R_h
Death & emigration
DR
e
Death & emigration
DR
e
Death & emigration
DR
e
Death & emigration
DR
e

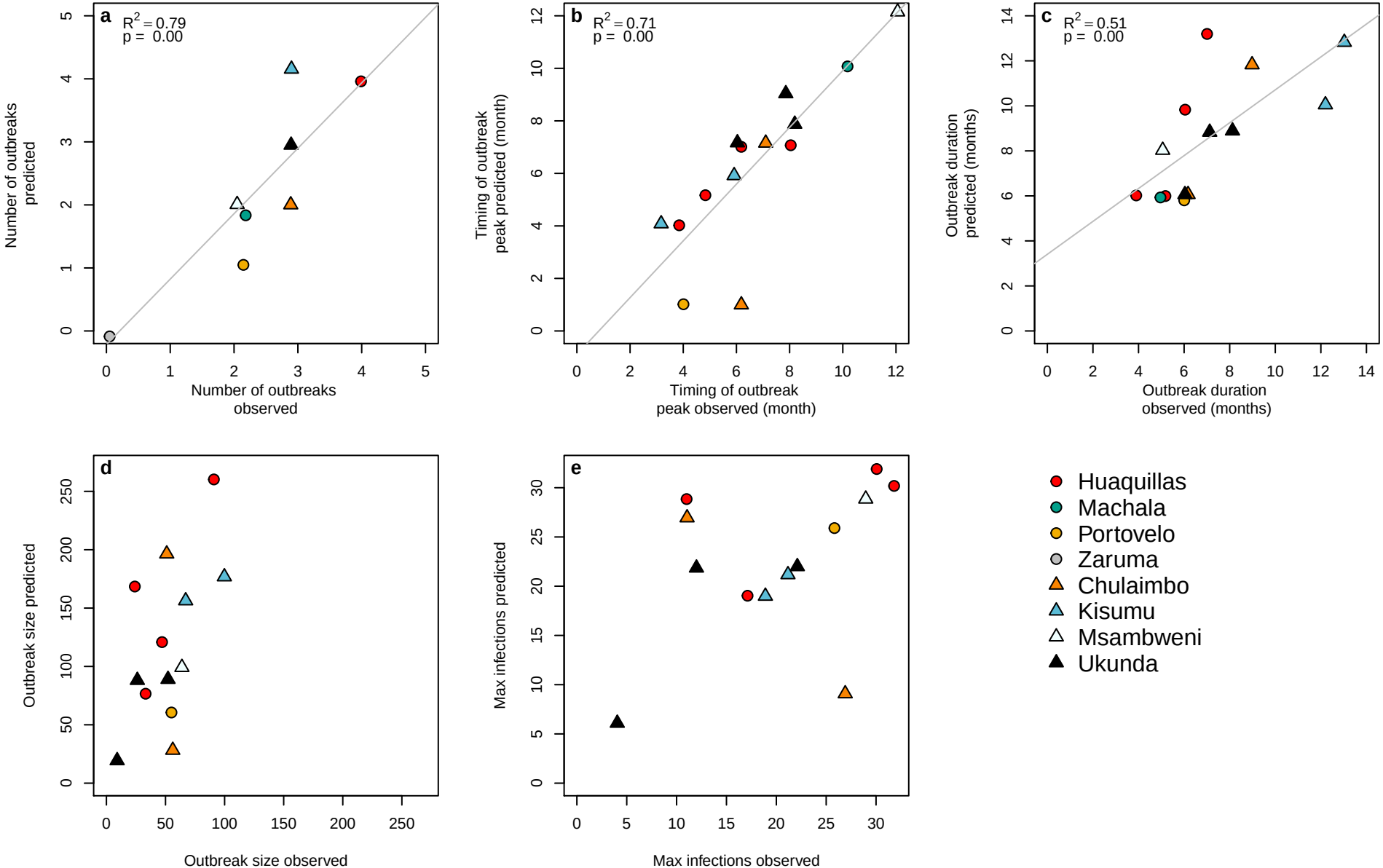
a
$R^2 = 0.79$
p = 0.00
Number of outbreaks predicted
Number of outbreaks observed
b
$R^2 = 0.71$
p = 0.00
Timing of outbreak peak predicted (month)
Timing of outbreak peak observed (month)
c
$R^2 = 0.51$
p = 0.00
Outbreak duration predicted (months)
Outbreak duration observed (months)
d
Outbreak size predicted
Outbreak size observed
e
Max infections predicted
Max infections observed
Huaquillas
Machala
Portovelo
Zaruma
Chulaimbo
Kisumu
Msambweni
Ukunda

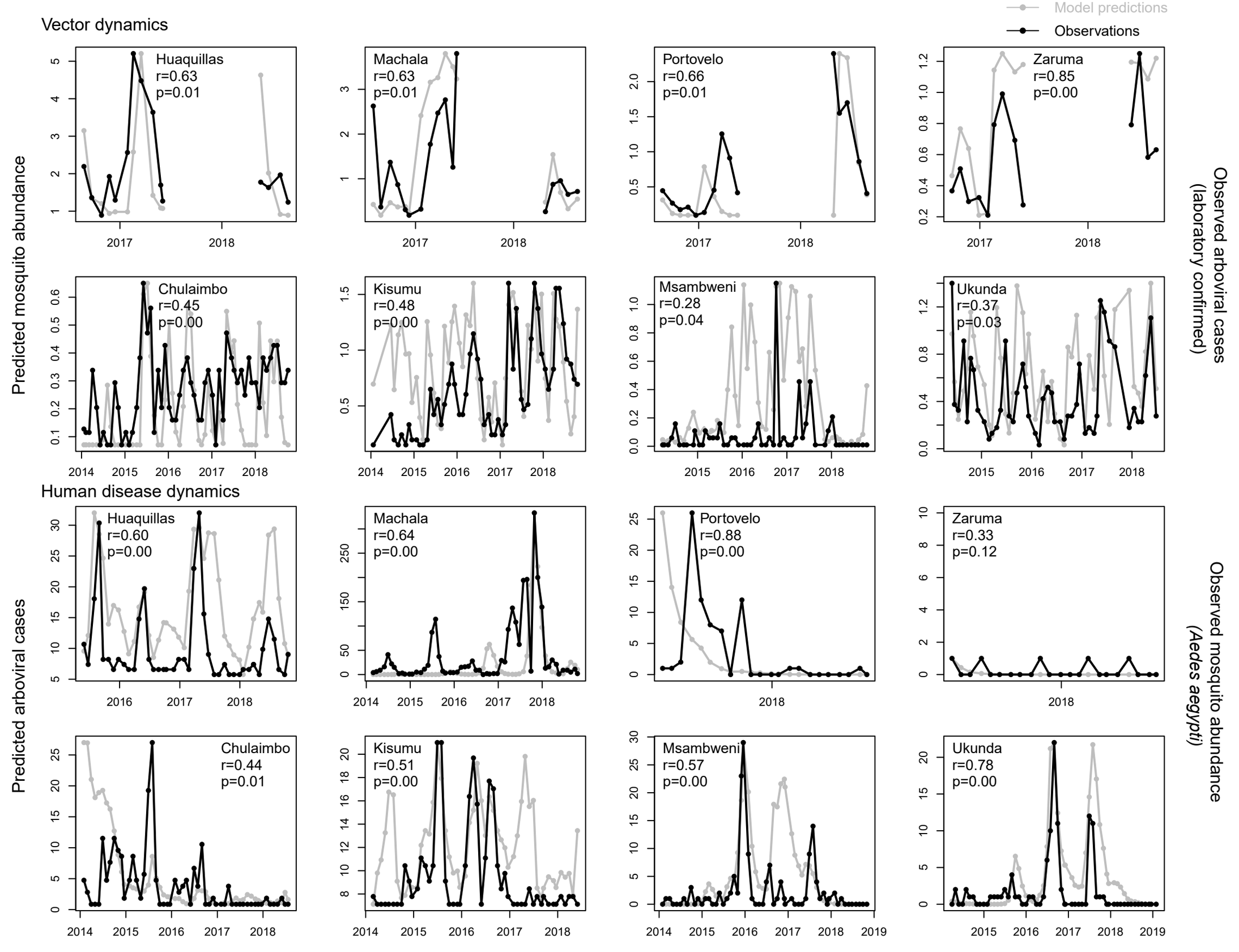
Model predictions
Observations
Vector dynamics
Predicted mosquito abundance
Observed arboviral cases
(laboratory confirmed)
Huaquillas
r=0.63
p=0.01
Machala
r=0.63
p=0.01
Portovelo
r=0.66
p=0.01
Zaruma
r=0.85
p=0.00
Chulaimbo
r=0.45
p=0.00
Kisumu
r=0.48
p=0.00
Msambweni
r=0.28
p=0.04
Ukunda
r=0.37
p=0.03
Human disease dynamics
Predicted arboviral cases
Observed mosquito abundance
(Aedes aegypti)
Huaquillas
r=0.60
p=0.00
Machala
r=0.64
p=0.00
Portovelo
r=0.88
p=0.00
Zaruma
r=0.33
p=0.12
Chulaimbo
r=0.44
p=0.01
Kisumu
r=0.51
p=0.00
Msambweni
r=0.57
p=0.00
Ukunda
r=0.78
p=0.00

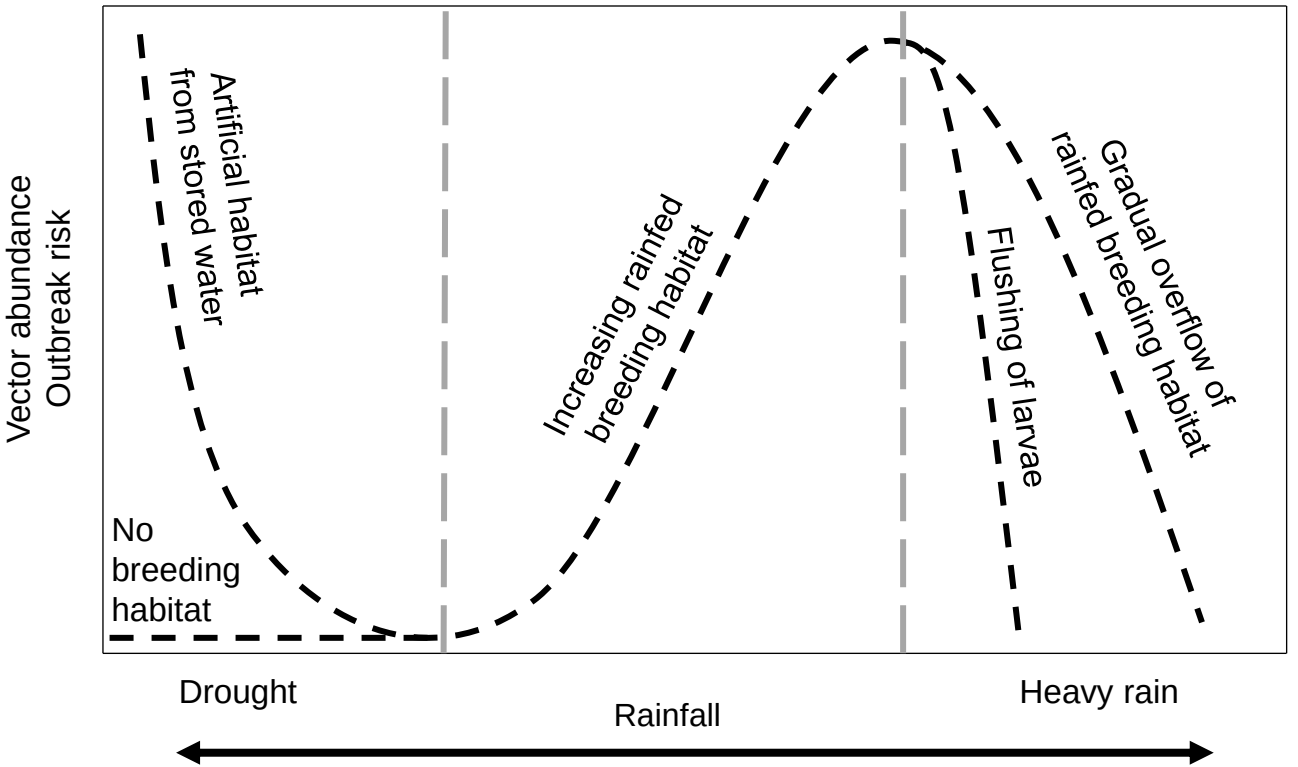
Vector abundance
Outbreak risk
Artificial habitat from stored water
No breeding habitat
Increasing rainfed breeding habitat
Flushing of larvae
Gradual overflow of rainfed breeding habitat
Drought
Rainfall
Heavy rain

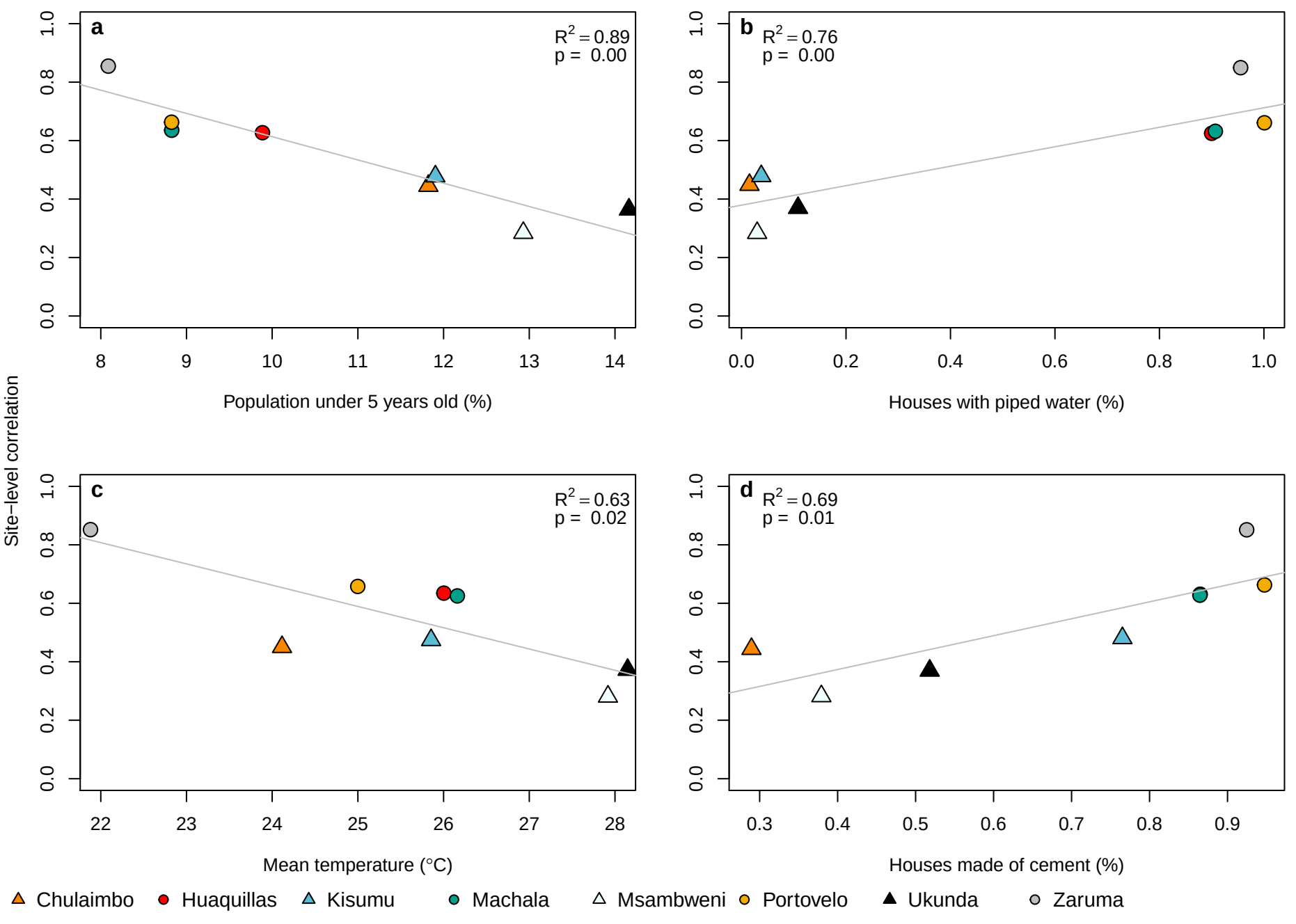
a
$R^2 = 0.89$
p = 0.00
b
$R^2 = 0.76$
p = 0.00
c
$R^2 = 0.63$
p = 0.02
d
$R^2 = 0.69$
p = 0.01
Site−level correlation
Population under 5 years old (%)
Houses with piped water (%)
Mean temperature (°C)
Houses made of cement (%)
Chulaimbo
Huaquillas
Kisumu
Machala
Msambweni
Portovelo
Ukunda
Zaruma

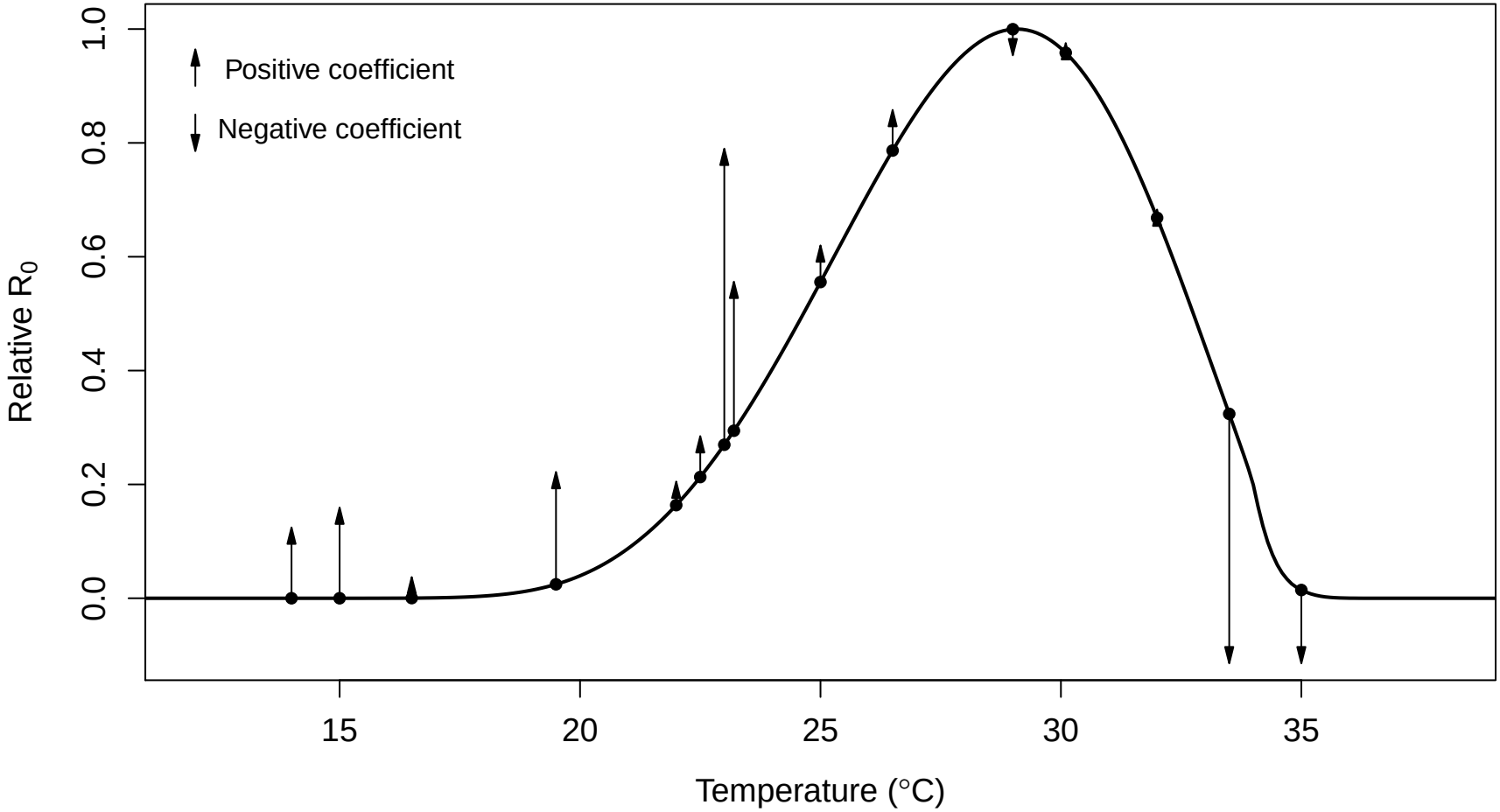
Positive coefficient
Negative coefficient
Relative R_0
0.0
0.2
0.4
0.6
0.8
1.0
15
20
25
30
35
Temperature (°C)